



1     **Variability of vertical structure of precipitation with sea surface temperature over the**  
2             **Arabian Sea and the Bay of Bengal as inferred by TRMM PR measurements**

3                     **Kadiri Saikranthi<sup>1</sup>, Basivi Radhakrishna<sup>2</sup>, Thota Narayana Rao<sup>2</sup> and**

4                                     **Sreedharan Krishnakumari Satheesh<sup>3</sup>**

5     <sup>1</sup> *Department of Earth and Climate Science, Indian Institute of Science Education and*  
6     *Research (IISER), Tirupati, India.*

7     <sup>2</sup> *National Atmospheric Research Laboratory, Department of Space, Govt. of India, Gadanki*  
8     *- 517112, India.*

9     <sup>3</sup> *Divecha Centre for Climate Change, Centre for Atmospheric and Oceanic Sciences, Indian*  
10    *Institute of Science, Bangalore - 560012, India.*

11

12

13

14

15

16

17

18

19

20

21

22

23

24

25

26

27

28

29

30

31

32

33

34

35

36

**Address of the corresponding author**

Dr. K. Saikranthi,  
Department of Earth and Climate Science,  
Indian Institute of Science Education and Research (IISER),  
Tirupati,  
Andhra Pradesh, India.  
Email: [ksaikranthi@gmail.com](mailto:ksaikranthi@gmail.com)



37 **Abstract**

38 Tropical Rainfall Measuring Mission (TRMM) Precipitation Radar (PR) 2A25  
39 reflectivity profiles data during the period 1998 - 2013 are used to study the differences in the  
40 vertical structure of precipitation and its variation with sea surface temperature (SST) over  
41 the Arabian Sea (AS) and the Bay of Bengal (BOB). Even though the AS and the BOB are  
42 parts of the Indian Ocean, they exhibit distinct features in vertical structure of precipitation  
43 and its variation with SST. The variation of reflectivity and precipitation echo top occurrence  
44 with SST is remarkable over the AS but trivial over the BOB. The median reflectivity  
45 increases with SST at all heights below 10 km altitude, but the increase is prominent below  
46 the freezing level height over the AS. On the other hand, irrespective of altitude, reflectivity  
47 profiles are same at all SSTs over the BOB. To understand these differences, variation of  
48 aerosols, cloud and water vapor with SST is studied over these seas. At SSTs less than 27°C,  
49 the observed high aerosol optical depth (AOD) and low total column water vapor (TCWV)  
50 over the AS results in small Cloud effective radius (CER) values and low reflectivity. As SST  
51 increases AOD decreases and TCWV increases, which result in large CER and high  
52 reflectivity. Over the BOB the change in AOD, TCWV and CER with SST is marginal. Thus,  
53 the observed variations in reflectivity profiles seem to be present from the cloud formation  
54 stage itself over both the seas.

55  
56  
57  
58  
59  
60  
61  
62  
63



## 64 **1. Introduction**

65 Indian summer monsoon (ISM) is one of the most complex weather phenomena,  
66 involving coupling between the atmosphere, land and ocean. At the boundary of the ocean  
67 and atmosphere air-sea interactions play a key role for the coupled Earth system (Wu and  
68 Kirtman 2005; Feng et al. 2018). SST – precipitation relations are the important measures for  
69 the air-sea interactions on different temporal scales (Woolnough et al., 2000; Rajendran et al.  
70 2012). Recent studies (Wang et al. 2005; Rajeevan et al. 2012; Chaudhari et al. 2013;  
71 Chaudhari et al. 2016) have shown that the simulation of ISM can be improved with the exact  
72 representation of sea surface temperature (SST) - precipitation relationship.

73 The dynamics of Madden-Julian oscillation (MJO) campaign (DYNAMO) portrayed  
74 the importance of understanding the link between SST and convective initiation at MJO  
75 scales (Yoneyama et al. 2013). With known differences in SST between Western Pacific and  
76 Indian Ocean, Barnes and Houze (2013) showed the occurrence of shallow systems  
77 maximized during the suppressed phases of MJO while the deep wide convective systems  
78 occurred during the active phases of MJO. SST modulates the meteorological factors that  
79 influence the formation and evolution of different kinds of precipitating systems over tropical  
80 oceans (Gadgil et al. 1984; Schumacher and Houze, 2003; Oueslati and Bellon 2015).

81 The relationships between the SST and cloud/precipitation have been studied in  
82 variety of contexts during the past three decades. The non-linear relationship of SST-  
83 precipitation/cloud occurrence (Gadgil et al. 1984; Woolnough et al., 2000; Rajendran et al.  
84 2012; Sabin et al. 2012; Meenu et al. 2012; Nair and Rajeev 2014; Roxy 2014; Nair et al.  
85 2017) is well documented over the Indian Ocean. The probability of organized convection  
86 increases with SST up to a critical value of  $\sim 28^{\circ}\text{C}$  (Gadgil et al. 1984). Sabin et al. (2012)  
87 and Meenu et al. (2012) showed that the convection is no longer dependent on SST at SSTs  
88 greater than  $30^{\circ}\text{C}$ . Later, by considering the time lag between the SST and rainfall Roxy



89 (2014) argued that this upper threshold can exceed till 31°C. Sengupta et al. (2001) showed  
90 that the intraseasonal variability of SST is not same over the entire Indian Ocean. Later, Roxy  
91 et al. (2013) estimated the time lag for SST and precipitation to be 2 and 5 weeks for the Bay  
92 of Bengal (BOB) and the Arabian Sea (AS), respectively. Through this study they found that  
93 the response of precipitation to SST anomalies is faster over the AS than the BOB. Also, the  
94 summer monsoon experiment (MONEX) showed the influence of the AS and the BOB on the  
95 rainfall produced over the Indian sub-continent (Krishnamurti 1985; Houze and Churchill  
96 1987) and also proved how these two seas are different with respect to the other oceans in  
97 terms of SST, back ground atmosphere and the occurrence of precipitating systems.

98         Knowing the differences in atmospheric conditions over the AS and the BOB during  
99 June and September (JJAS) the occurrence of various kinds of precipitating systems over  
100 these two seas is studied in Liu et al. (2007), Romatschke et al. (2010), Saikranthi et al.  
101 (2014), Houze et al. (2015). These studies showed that the occurrence of shallow systems is  
102 prevalent over the Arabian Sea while deeper systems are abundant in the Bay of Bengal.  
103 Recently, Saikranthi et al. (2018) showed that the observed differences in the occurrence of  
104 various kinds of precipitating systems is exist even in El Niño and La Niña periods also, but  
105 with variable magnitudes. Aforementioned studies mainly focussed on the variation of  
106 surface rainfall, morphology of vertical structure of precipitation, occurrence of cloudiness  
107 with SST over the Indian Ocean. But, none of them studied the variation of vertical structure  
108 of precipitation (in terms of occurrence and intensity) with SST. The strength of the  
109 convective forcing strongly depends on SST (Sabin et al. 2012) and changes in SST have the  
110 potential of altering the vertical structure of precipitation (Oueslati and Bellon 2015).

111         The vertical structure of precipitation information is essential for improving the  
112 accuracy of rainfall estimation (Fu and Liu 2001; Sunilkumar et al. 2015), understanding the  
113 dynamical and microphysical processes of hydrometeor growth/decay mechanisms (Houze



114 2004; Greets and Dejene 2005; Saikranthi et al. 2014; Rao et al. 2016) and flash rates (Liu et  
115 al. 2012), and for improving the latent heating retrievals (Tao et al. 2006). Also, most of the  
116 earlier studies dealing with SST and cloud/precipitation population considered whole Indian  
117 ocean as a single entity. But in reality the BOB and the AS of Indian ocean possesses  
118 distinctly different features, like SST and its variability over seasonal and intraseasonal scales  
119 (Sengupta et al. 2001; Roxy et al. 2013), the monsoonal wind speeds (Findlater 1969) and  
120 also the type of rain (Liu et al. 2007; Romatschke et al. 2010; Saikranthi et al. 2014; Rao et  
121 al. 2016). Knowing the importance of vertical structure of precipitation and SST modulation  
122 of background atmospheric conditions, in the present study we have studied the variation of  
123 vertical structure of precipitation with SST and their causative mechanisms over different  
124 regions of Indian ocean, in particular over the BOB and the AS.

125 The present paper is organized as follows. Section 2 describes the data and method of  
126 analysis. The variation of the vertical structure of precipitation with SST over BOB and AS is  
127 studied in section 3. Section 4 discusses the factors influencing the variation of vertical  
128 structure over BOB and AS. The results are summarized in Section 5.

## 129 **2. Data**

130 The present study utilizes 16 years (1998-2013) of Tropical rainfall measuring  
131 mission (TRMM) precipitation radar (PR) 2A25 (version 7) dataset during the southwest  
132 monsoon season (June to September). TRMM-PR dataset comprising vertical profiles of  
133 attenuation corrected reflectivity with 17 dBZ as minimum detectable signal (Iguchi et al.  
134 2009). Comparing TRMM-PR data with Kwajalein S-band radar data Schumacher and Houze  
135 (2000) showed that TRMM-PR misses 15% of the echo area observed above 0°C levels due  
136 to the sensitivity threshold (17 dBZ). Through this study they concluded that TRMM-PR  
137 highly under samples weaker echoes from ice particles associated with stratiform rain aloft  
138 but manages to capture most of the near-surface precipitation accumulation. The range



139 resolution of TRMM-PR reflectivity profiles is 250 m with a horizontal footprint size of ~4.3  
140 and 5 km before and after the boosting of its orbit, respectively. It scans  $\pm 17^\circ$  from nadir with  
141 a beam width of  $0.71^\circ$  covering a swath of 215 km (245 km after the boost). TRMM-PR data  
142 uniqueness is its ability in pigeonholing the precipitating systems into convective, stratiform  
143 and shallow rain. This classification is based on two methods namely the horizontal method  
144 (H - method) and the vertical method (V - method) using the bright band identification and  
145 the reflectivity profile (Awaka et al. 2009). The original TRMM-PR 2A25 vertical profiles of  
146 attenuation corrected reflectivity are gridded to a three dimensional Cartesian coordinate  
147 system with a spatial resolution of  $0.05^\circ \times 0.05^\circ$ . The detailed methodology of interpolating  
148 the TRMM-PR reflectivity data into the 3D Cartesian grid is discussed in Houze et al. (2007).  
149 This dataset is available at the University of Washington website  
150 (<http://trmm.atmos.washington.edu/>).

151 To understand the observed variations in the vertical structure of precipitation in the  
152 light of microphysics of clouds, Moderate Resolution Imaging Spectroradiometer (MODIS)  
153 AQUA satellite level 3 data (MYD08) are considered. In particular, the daily atmospheric  
154 products of aerosol optical depth (AOD) (Hubanks et al. 2008), cloud effective radius (CER)  
155 ice, and CER liquid (Platnick et al. 2017) during the period 2003 and 2013 have been used.  
156 MODIS AOD dataset is a collection of aerosol optical properties at 550 nm wavelength, as  
157 well as particle size information. Level 2 MODIS AOD is derived from radiances using either  
158 one of the three different algorithms, i.e., over ocean Remer et al. (2005) algorithm, over land  
159 the Dark-Target (Levy et al. 2007) algorithm and for brighter land surfaces the Deep-Blue  
160 (Hsu et al. 2004) algorithm. CER is nothing but the weighted mean of the size distribution of  
161 cloud drops i.e., the ratio of third moment to second moment of the drop size distribution. In  
162 the level 3 MODIS daily dataset, aerosol and cloud products of level 2 data pixels with valid  
163 retrievals within a calendar day are first aggregated and gridded to a daily average with a



164 spatial resolution of  $1^\circ \times 1^\circ$ . For CER grid box values, CER values are weighted by the  
165 respective ice/liquid water cloud pixel counts for the spatiotemporal aggregation and  
166 averaging processes.

167 The background atmospheric structure and SST information are taken from the  
168 European Centre for Medium Range Weather Forecasting (ECMWF) Interim Reanalysis  
169 (ERA). ERA-Interim runs 4DVAR assimilation twice daily (00 and 12 UTC) to determine the  
170 most likely state of the atmosphere at a given time (analysis). The consistency across  
171 variables in space and in time (during 12-hour intervals) is thus ensured by the atmospheric  
172 model and its error characteristics as specified in the assimilation. ERA-Interim is produced  
173 at T255 spectral resolution (about  $0.75^\circ$ ,  $\sim 83$  km) with a temporal resolution of 6h for upper  
174 air fields and 3h for surface fields. The performance of the data assimilation system and the  
175 strengths and limitations of ERA-Interim datasets are found in Dee et al. (2011). The original  
176  $0.75^\circ \times 0.75^\circ$  spatial resolution gridded dataset is rescaled to a resolution of  $0.125^\circ \times 0.125^\circ$ .  
177 The temporal resolution of the dataset used is 6h (00, 06, 12 and 18 UTC).

178 The variation of vertical structure of precipitation with SST are studied by considering  
179 the dataset between  $63^\circ\text{E} - 72^\circ\text{E}$  and  $8^\circ\text{N} - 20^\circ\text{N}$  over the AS and  $83^\circ\text{E} - 92^\circ\text{E}$  and  $8^\circ\text{N} - 21^\circ\text{N}$   
180 over the BOB. These regions of interest along with the SWM seasonal mean SST over the  
181 two seas are depicted in Fig. 1. These regions are selected in such a way that the coastal  
182 influence on SST is eluded from the analysis. As small amount of rainfall is observed over  
183 the western AS (west to  $63^\circ\text{E}$  latitude) during SWM (Saikranthi et al. 2018), this region is  
184 also not considered in the present analysis. The seasonal mean SST is higher over the BOB  
185 than in the AS by more than  $1^\circ\text{C}$  during the SWM season corroborating the findings of  
186 Shenoi et al. (2002). The nearest space and time matched SST data from ERA-Interim are  
187 assigned to the TRMM-PR and MODIS observations for further analysis.



### 189 3. Variation of vertical structure of precipitation with SST

190 The occurrence (in terms of %) of conditional precipitation echoes ( $Z \geq 17$  dBZ) at  
191 different altitudes as a function of SST over the AS and the BOB is shown in Fig. 2. The  
192 variation of precipitation echoes occurrence frequency with SST is quite different over both  
193 the seas. It increases with increase in SST over the AS, but remains nearly same over the  
194 BOB. Higher occurrence of precipitation extends to higher heights with increasing SST over  
195 the AS, while such variation is not quite evident over the BOB. Precipitation echoes are  
196 confined to 8 km at lower SST ( $< 28^\circ$  C) over the AS, but exhibits a gradual rise in height  
197 with increase in SST. Confinement of echoes to lower heights at lower SST is mainly due to  
198 the abundant occurrence of shallow systems over the AS (Saikranthi et al. 2014; Rao et al.  
199 2016). Interestingly, high occurrence of precipitation is seen at higher heights even at lower  
200 SSTs over the BOB, indicating the presence of deeper storms. Such systems exist at all SST's  
201 over the BOB.

202 To examine the variation of reflectivity profiles with SST, median profiles of  
203 reflectivity in each SST bin are computed over the AS and the BOB and are depicted in Figs.  
204 3a & 3d, respectively. The space- and time-matched conditional reflectivity profiles are  
205 grouped into  $1^\circ$ C SST bins and then the median is estimated at each height, only if the  
206 number of conditional reflectivity pixels (Figs. 3c & 3f) is greater than 500. It is clear from  
207 Figs. 3a & 3d that the median reflectivity profiles are distinctly different over the AS and the  
208 BOB, even at same SST. Over the AS, reflectivity profiles show only small variations ( $\leq 1$   
209 dBZ) with SST above ( $> 5$  km) the melting region, but vary significantly below the melting  
210 level ( $< 5$  km). These variations in reflectivity profiles with SST are negligible over the BOB.  
211 Below the melting layer, the reflectivity increases from 24 dBZ to  $\sim 28$  dBZ with increase in  
212 SST from  $26^\circ$ C to  $30^\circ$ C over the AS, but it is almost the same ( $\sim 28$ dBZ) at all SST's over  
213 the BOB. The standard deviation of reflectivity also exhibits similar variation as that of



214 median profiles with SST over the AS and the BOB. In general the standard deviation of  
215 reflectivity, representing the variability in reflectivity within the SST bin, is larger over the  
216 BOB than the AS.

217         The median reflectivity profiles show a gradual increase with decreasing altitude from  
218 ~ 10 km to 6 km and an abrupt enhancement is seen just below 6 km over both the seas. The  
219 sudden enhancement at the freezing level is primarily due to the aggregation of hydrometeors  
220 and change in dielectric factor from ice to water (Fabry and Zawadzki 1995; Rao et al. 2008;  
221 Cao et al. 2013). Below the bright band, the raindrops can grow by collision-coalescence  
222 process and reduce their size either by breakup or by evaporation processes. The collision -  
223 coalescence results in negative slope in the reflectivity profile, whereas breakup and  
224 evaporation results in positive slope (Liu and Zipser 2013; Cao et al. 2013; Saikranthi et al.  
225 2014). The observed negative slope in the median reflectivity profiles below the bright band  
226 region indicates the low-level hydrometeor growth over both the seas. This hydrometeor  
227 growth below melting region indicates the predominance of collision-coalescence process  
228 than the collision-breakup process over both the seas. The magnitude of the slope is nearly  
229 equal over both the seas, indicating that the rate of growth, on average, is nearly equal.

#### 230 **4. Factors affecting the vertical variation of reflectivity with SST**

231         The formation and evolution of precipitating systems depends on the stability of the  
232 boundary layer, dynamics and thermodynamics of the ambient atmosphere. To know the  
233 stability of the marine boundary layer at various SSTs the lower tropospheric stability (LTS)  
234 is considered. LTS is defined as the difference in potential temperature between 700 hPa  
235 ( $\theta_{700}$ ) and surface ( $\theta_0$ ) i.e.,  $LTS = \theta_{700} - \theta_0$  that represents the strength of the inversion caps by  
236 the planetary boundary layer (Wood and Bretherton 2006). The LTS values were computed  
237 from the ERA-Interim temperature data during SWM season over the selected regions and  
238 are depicted in Fig. 4(a). LTS decreases with SST up to 29°C and increases a little at further



239 SSTs over both the seas however when compared to the BOB the LTS values are larger over  
240 the AS at all SSTs. The stability of the planetary boundary layer is very high at lower SSTs  
241 and as SST increases the stability decreases drastically over the AS up to 29°C and increases  
242 a little at further SSTs. On the other hand the variability in planetary boundary layer stability  
243 with SST is trivial over the BOB. Also shown in Fig. 4(b) is the convective available  
244 potential energy (CAPE) at different SSTs over both the Seas. CAPE is calculated following  
245 Emanuel (1994). CAPE increases with rise in SST over both the seas while its magnitude is  
246 relatively large over the BOB than the AS at all SSTs. The large LTS and small CAPE values  
247 at lower SSTs over the AS don't allow the precipitating systems to grow to higher altitudes  
248 and in turn precipitate in the form of warm rain. As SST increases LTS decreases drastically  
249 and CAPE increases and hence the precipitating systems can grow to higher altitudes.  
250 Though LTS increases above 29°C the instability created by the large CAPE can penetrate  
251 the planetary boundary layer and favours the formation of deeper systems. On the other hand  
252 LTS values are lower and remain almost same at all SSTs and large CAPE values over the  
253 BOB are conducive for the precipitating systems to grow to higher altitudes as depicted in  
254 Fig. 2.

255         The observed differences in reflectivity profiles of precipitation with SST could be  
256 originated at the cloud formation stage or in the evolution stage or due to both. In order to  
257 understand this, the variation of mean CER for ice and liquid at different SST's over the AS  
258 and the BOB is depicted in Figs. 5a & 5b, respectively. The mean is calculated only when the  
259 number of data points is larger than 100 in each SST bin. It is evident from Figs. 5a & 5b that  
260 both CER ice and liquid increase with rise in SST substantially over the AS but the increase  
261 is marginal over the BOB. For example, as SST rises from 26°C to 31°C, the CER ice and  
262 liquid vary from 20  $\mu\text{m}$  to 32  $\mu\text{m}$  and 14.7  $\mu\text{m}$  to 20.8  $\mu\text{m}$ , respectively over the AS, whereas  
263 they vary, respectively, from 29  $\mu\text{m}$  to 31  $\mu\text{m}$  and 18.5  $\mu\text{m}$  to 19.5  $\mu\text{m}$  over the BOB. Also,



264 the cloud droplets are small in size at lower SSTs and bigger at higher SSTs over the AS,  
265 whereas they are big over the BOB irrespective of SST. These smaller sized hydrometeors at  
266 low SSTs are responsible for the observed small reflectivities above the melting layer over  
267 the AS than the BOB as reflectivity is more sensitive to the particle size than the droplet  
268 concentration ( $Z \propto D^6$ ). At higher SSTs, the CER values are approximately equal over both  
269 the seas and in turn the observed reflectivities (Fig. 5). This suggests that the variations seen  
270 in vertical profiles of reflectivity are originating in the cloud itself.

271 Numerous studies have examined the aerosol effects on cloud formation through  
272 heterogeneous nucleation and precipitation (Twomey 1977; Albrecht 1989; Tao et al. 2012;  
273 and Rosenfeld et al. 2014). For fixed liquid water content, as the concentration of aerosols  
274 increases, the number of cloud drops increases and droplet size reduces (Twomey 1977).  
275 Utilizing the aircraft measurements over Indian sub-continent Ramanathan et al. (2001)  
276 showed that the cloud drop number density increase with increasing aerosol number density  
277 both over continental and maritime regions. Connolly et al. (2009), Li and Min (2010),  
278 Niemand et al. (2012), Creamean et al. (2013), and Fan et al. (2014) showed that dust also  
279 act as ice nuclei through heterogeneous nucleation and these ice nuclei directly change the ice  
280 nucleation processes that determine the initial number concentration and size distribution of  
281 ice crystals. Thus, to understand the role of aerosols in the observed variations in the CER  
282 with SST, the seasonal mean AOD variation with SST is plotted in Fig. 6a for the SWM.  
283 AOD decreases from 0.62 to 0.31 with rise in SST from 26°C to 31°C over the AS but only  
284 0.42 to 0.36 as SST varies from 27°C to 30°C and then increases with rise in SST over the  
285 BOB. Also shown in Fig. 6b is the variation of total column water vapor (TCWV) with SST  
286 over both the seas. TCWV shows a gradual increase with SST over the AS while it decreases  
287 initially from 27°C to 28°C, and then increases with SST over the BOB. At a given SST the  
288 TCWV is more in the BOB than in the AS. More number of aerosols and relatively low



289 TCWV over the AS results in large number of cloud drops with reduced size (Twomey 1977;  
290 Ramanathan 2001). These reduced size cloud drops are responsible for the observed small  
291 CER values at SSTs less than 28°C. As SST rises the AOD decreases and TCWV increases  
292 such that the cloud particles grow in size which in turn increases CER. On the other hand, the  
293 change in AOD and TCWV (and as a result in CER) is not prominent with SST over the  
294 BOB, as seen in the Fig. 5.

295 To understand the transport of aerosols at low and mid-levels the wind magnitudes  
296 and directions at 850 hPa and 500 hPa levels are shown in Fig. 7. The strong lower  
297 tropospheric winds produce sea salt particles as well as transport dust from the Horn of  
298 Africa and the mid tropospheric winds transport dust from the Arabian Desert over the AS  
299 (Li and Ramanathan 2002). On the other hand the continental aerosols from India landmass  
300 are transported to the BOB both at low and mid troposphere. Satheesh et al. (2006) showed  
301 an increase in AOD with increase in latitude over the AS due to the dust advection from  
302 Arabia desert regions during SWM season, whereas SST decreases with increase in the  
303 latitude. In other words the SST is low and AOD is high in northern AS whereas over the  
304 southern AS, SST is high and AOD is low. This contrasting spatial distribution of AOD and  
305 SST could cause a negative correlation between AOD and SST. To examine whether the  
306 observed decrease in AOD with increase in SST over the AS is due to the latitudinal variation  
307 of AOD or exists at all latitudes, we have segregated the data into 2° latitude bins and plotted  
308 the mean AOD with SST for all bins and is depicted in Fig. 8a. In spite of the magnitude,  
309 AOD variation with SST is nearly similar at all latitudes of the AS, i.e., the higher AOD is  
310 observed at lower SSTs and vice versa. On the other hand the latitudinal variation of AOD  
311 with SST over the BOB shown in Fig. 8b also show a decrease in AOD with SST up to 30°C  
312 but the magnitude of variation is trivial relative to the AS. As also depicted in Fig. 6a above  
313 30°C AOD increases with SST over the BOB. This indicates that though there is a difference



314 in magnitude of variation, AOD varies with SST over both the seas at all latitudes. This  
315 analysis is repeated using the multi-angle imaging spectroradiometer (MISR) dataset (which  
316 is not shown here) for small, medium large aerosol particles. Interestingly all three types also  
317 show a decrease in AOD with rise in SST over both the seas.

## 318 **5. Conclusions**

319 Sixteen years of TRMM-PR 2A25 reflectivity profiles and 11 years of MODIS AOD  
320 and CER data are utilized to understand the differences in variation of vertical structure of  
321 precipitation with SST over AS and BOB. This analysis reveals that the variation of  
322 reflectivity with SST is remarkable over the AS and marginal over the BOB. The reflectivity  
323 increases with rise in SST over the AS and remains the same at all SSTs over the BOB. This  
324 change in reflectivity over the AS is more prominent below the freezing level height (~ 4  
325 dBZ) than the above (~ 1 dBZ). Over the AS, the abundance of aerosols and less moisture at  
326 SSTs < 27°C result in high concentration of small diameter cloud droplets. As SST increases  
327 the aerosol concentration decreases and moisture increases such that the bigger cloud droplets  
328 are formed. Thus, the reflectivity increases with rise in SST over the AS. On the other hand,  
329 AOD, TCWV and CER do not show substantial variation with SST over the BOB and hence  
330 the change in reflectivity is small. Over the BOB, the mid troposphere is wet and  
331 hydrometeor's size at the formation stage is nearly the same at all SSTs. The evolution of  
332 hydrometeors during their descent is also similar at all SST's, as evidenced by nearly similar  
333 reflectivity profiles.

## 334 **Acknowledgements**

335 The authors would like to thank Prof. Robert Houze and his team for the interpolated 3D  
336 gridded TRMM-PR dataset (<http://trmm.atmos.washington.edu>), ECMWF (<http://data-portal.ecmwf.int/>) team for providing the ERA-Interim dataset and MODIS  
337 (<https://ladsweb.modaps.eosdis.nasa.gov/>) science team for providing the AOD and CER



339 dataset. The authors express their gratitude to Prof. J. Srinivasan for his fruitful discussions  
340 and valuable suggestions in improving the quality of the manuscript. The corresponding  
341 author would like to thank Department of Science & Technology (DST), India for providing  
342 the financial support through the reference number DST/INSPIRE/04/2017/001185.

### 343 **References**

344 Albrecht, B.A.: Aerosols, cloud microphysics, and fractional cloudiness, *Science*, 245, 1227–  
345 1230, 1989.

346 Awaka, J., Iguchi, T., and Okamoto, K.: TRMM PR standard algorithm 2A23 and its  
347 performance on bright band detection, *J. Meteorol. Soc. Jpn.*, 87A, 31–52, 2009.

348 Barnes, H. C., and Houze, Jr. R. A.: The precipitating cloud population of the Madden-Julian  
349 oscillation over the Indian and West Pacific Oceans. *J. Geophys. Res.*, 118, 6996-7023,  
350 doi:10.1002/jgrd.50375, 2013.

351 Cao, Q., Hong, Y., Gourley, J. J., Qi, Y., Zhang, J., Wen, Y., and Kirstetter, P. E.: Statistical  
352 and physical analysis of the vertical structure of precipitation in the mountainous west  
353 region of the United States using 11+ years of space borne observations from TRMM  
354 precipitation radar, *J. Appl. Meteorol. Climatol.*, 52, 408-424, 2013.

355 Chaudhari, H. S., Pokhrel, S., Mohanty, S., and Saha, S. K.: Seasonal prediction of Indian  
356 summer monsoon in NCEP coupled and uncoupled model, *Theor. Appl. Climatol.*, 114,  
357 459–477, doi:10.1007/s00704-013-0854-8, 2013.

358 Chaudhari, H. S., Pokhrel, S., Kulkarni, A., Hazra, A., and Saha, S. K.: Clouds-SST  
359 relationship and interannual variability modes of Indian summer monsoon in the  
360 context of clouds and SSTs: observational and modelling aspects, *Int. J. Climatol.*, doi:  
361 10.1002/joc.4664, 2016.



- 362 Connolly, P. J., Möhler, O., Field, P. R., Saathoff, H., Burgess, R., Choularton, T., and  
363 Gallagher, M.: Studies of heterogeneous freezing by three different desert dust samples.  
364 *Atmos. Chem. Phys.*, 9, 2805–2824, doi:10.5194/acp-9-2805-2009, 2009.
- 365 Creamean, J. M., Suski, K. J., Rosenfeld, D., Cazorla, A., DeMott, P. J., Sullivan, R. C.,  
366 White, A. B., Ralph, F. M., Minnis, P., Comstock, J. M., Tomlinson, J. M., Kimberly  
367 A., and Prather, K. A.: Dust and biological aerosols from the Sahara and Asia influence  
368 precipitation in the western U.S., *Science*, 339, 1572–1578,  
369 doi:10.1126/science.1227279, 2013.
- 370 Dee, D. P., et al.: The ERA-Interim reanalysis: Configuration and performance of the data  
371 assimilation system, *Q. J. R. Meteorol. Soc.*, 137, 553–597, 2011.
- 372 Emanuel, K. A.: Atmospheric convection. Oxford University Press, Oxford, 1994.
- 373 Fabry, F., and Zawadzki, I.: Long-term radar observations of the melting layer of  
374 precipitation and their interpretation, *J. Atmos. Sci.*, 52, 838–851, 1995.
- 375 Fan, J., Leung, L. R., DeMott, P. J., Comstock, J. M., Singh, B., Rosenfeld, D., Tomlinson, J.  
376 M., White, A., Prather, K. A., Minnis, P., Ayers, J. K., and Min, Q.: Aerosol impacts on  
377 California winter clouds and precipitation during CalWater 2011: local pollution versus  
378 long-range transported dust, *Atmos. Chem. Phys.*, 14, 81–101,  
379 <https://doi.org/10.5194/acp-14-81-2014>, 2014.
- 380 Feng, X., Haines, K., Liu, C., de Boissésou, E., and Polo, I., Improved SST-precipitation  
381 intraseasonal relationships in the ECMWF coupled climate reanalysis, *Geophys. Res.  
382 Lett.*, 45, 3664–3672, 2018.
- 383 Findlater, J.: A major low-level air current near the Indian Ocean during the northern  
384 summer, *Q. J. R. Meteorol. Soc.*, 95, 362–380, 1969.



- 385 Fu, Y., and Liu, G.: The variability of tropical precipitation profiles and its impact on  
386 microwave brightness temperatures as inferred from TRMM data, *J. Appl. Meteorol.*,  
387 40, 2130–2143, 2001.
- 388 Gadgil, S., Joseph, P. V., and Joshi, N. V.: Ocean atmosphere coupling over monsoonal  
389 regions, *Nature*, 312, 141–143, 1984.
- 390 Geerts, B., and Dejene, T.: Regional and diurnal variability of the vertical structure of  
391 precipitation systems in Africa based on space borne radar data, *J. Clim.*, 18, 893–916,  
392 2005.
- 393 Houze, R. A.: Mesoscale convective systems, *Rev. Geophys.*, 42, RG4003, doi:  
394 10.1029/2004RG000150, 2004.
- 395 Houze, R. A., and Churchill, D. D.: Mesoscale organization and cloud microphysics in a Bay  
396 of Bengal depression, *J. Atmos. Sci.*, 44, 1845–1867, 1987.
- 397 Houze, R. A., Wilton, D. C., and Smull, B. F.: Monsoon convection in the Himalayan region  
398 as seen by the TRMM precipitation radar, *Q. J. R. Meteorol. Soc.*, 133, 1389–1411,  
399 2007.
- 400 Houze, R. A., Rasmussen, K. L., Zuluaga, M. D., and Brodzik, S. R.: The variable nature of  
401 convection in the tropics and subtropics: A legacy of 16 years of the Tropical rainfall  
402 measuring mission satellite, *Rev. Geophys.*, 53, 994–1021, 2015.
- 403 Hsu, N., Tsay, S., King, M., and Herman, J.: Aerosol properties over bright-reflecting source  
404 regions, *Geosci. Remote Sens. IEEE Trans.*, 42, 557–569, 2004.
- 405 Hubanks, P., King, M., Platnick, S., and Pincus, R.: MODIS atmosphere L3 gridded product  
406 algorithm theoretical basis document collection 005 Version 1.1, Tech. Rep. ATBD-  
407 MOD-30, NASA, 2008.



- 408 Iguchi, T., Kozu, T., Kwiatkowski, J., Meneghini, R., Awaka, J., and Okamoto, K.:  
409       Uncertainties in the rain profiling algorithm for the TRMM precipitation radar, *J.*  
410       *Meteor. Soc. Japan*, 87A, 1–30, doi:10.2151/jmsj.87A.1, 2009.
- 411 Krishnamurti, T. N.: Summer monsoon experiment – A review. *Mon. Wea. Rev.*, **113**, 1590-  
412       1626, 1985.
- 413 Levy, R., Remer, L., Mattoo, S., Vermote, E., and Kaufman, Y.: Second-generation  
414       operational algorithm: Retrieval of aerosol properties over land from inversion of  
415       moderate resolution imaging spectroradiometer spectral reflectance, *J. Geophys. Res.*,  
416       112, D13, doi:10.1029/2006JD007811, 2007.
- 417 Li, F., and Ramanathan, V.: Winter to summer monsoon variation of aerosol optical depth  
418       over the tropical Indian Ocean, *J. Geophys. Res.*, 107(D16), doi:  
419       10.1029/2001JD000949, 2002.
- 420 Li, R., and Min, Q.-L.: Impacts of mineral dust on the vertical structure of precipitation. *J.*  
421       *Geophys. Res.*, 115, D09203, doi:10.1029/2009JD011925, 2010.
- 422 Liu, C., and Zipser, E. J.: Why does radar reflectivity tend to increase downward toward the  
423       ocean surface, but decrease downward toward the land surface?, *J. Geophys. Res.*  
424       *Atmos.*, 118, 135-148, doi: 10.1029/2012JD018134, 2013.
- 425 Liu, C., Zipser, E., and Nesbitt, S. W.: Global distribution of tropical deep convection:  
426       Different perspectives using infrared and radar as the primary data source, *J. Climate*,  
427       20, 489-503, 2007.
- 428 Liu, C., Cecil, D., and Zipser, E. J.: Relationships between lightning flash rates and radar  
429       reflectivity vertical structures in thunderstorms over the tropics and subtropics. *J.*  
430       *Geophys. Res.*, doi:10.1029/2011JD017123, 2012.



- 431 Meenu, S., Parameswaran, K., and Rajeev, K.: Role of sea surface temperature and wind  
432 convergence in regulating convection over the tropical Indian Ocean, *J. Geophys. Res.*  
433 *Atmos.*, 117, D14102, 2012.
- 434 Nair, A. K. M., and Rajeev, K.: Multiyear CloudSat and CALIPSO observations of the  
435 dependence of cloud vertical distribution on sea surface temperature and tropospheric  
436 dynamics, *J. Clim.*, 27, 672–683, doi:10.1175/JCLI-D-13-00062.1, 2014.
- 437 Nair, A.K.M., Rao, T. N., and Rajeev, K.: Role of cloud feedback in regulating the “pool of  
438 inhibited cloudiness” over the Bay of Bengal, *Meteorol. Atmos. Phys.*,  
439 <https://doi.org/10.1007/s00703-017-0560-7>, 2017.
- 440 Niemand, M., Möhler, O., Vogel, B., Vogel, H., Hoose, C., Connolly, P., Klein, H.,  
441 Bingemer, H., DeMott, P., Skrotzki, J., and Leisner, T.: A particle-surface-area-based  
442 parameterization of immersion freezing on desert dust particles, *J. Atmos. Sci.*, 69,  
443 3077–3092, <https://doi.org/10.1175/JAS-D-11-0249.1>, 2012.
- 444 Oueslati, B., and Bellon, G.: The double ITCZ bias in CMIP5 models: interaction between  
445 SST, large-scale circulation and precipitation. *Climate Dyn.*, 44, 585–607, 2015.
- 446 Platnick, S., et al.: The MODIS cloud optical and microphysical products: Collection 6  
447 updates and examples from Terra and Aqua, *IEEE Trans. Geosci. Remote Sens.*, 55,  
448 502–525, doi:10.1109/TGRS.2016.2610522, 2017.
- 449 Rajeevan, M., Unnikrishnan, C. K., and Preethi, B.: Evaluation of the ENSEMBLES multi-  
450 model seasonal forecasts of Indian summer monsoon variability, *Clim. Dyn.*, 38, 2257–  
451 2274, 2012.
- 452 Rajendran, K., Nanjundiah, R. S., Gadgil, S., and Srinivasan, J.: How good are the  
453 simulations of tropical SST–rainfall relationship by IPCC AR4 atmospheric and  
454 coupled models?, *J. Earth Sys. Sci.*, 121(3), 595–610, 2012.



- 455 Ramanathan, V., Crutzen, P. J., Kiehl, J. T., Rosenfeld, D.: Aerosols, climate, and the  
456 hydrological cycle, *Science*, 294, 2119-2124, 2011.
- 457 Rao, T. N., Kirankumar, N. V. P., Radhakrishna, B., Rao, D. N., and Nakamura, K.:  
458 Classification of tropical precipitating systems using wind profiler spectral moments.  
459 Part I: Algorithm description and validation, *J. Atmos. Oceanic Technol.*, 25, 884–897,  
460 2008.
- 461 Rao, T. N., Saikranthi, K., Radhakrishna, B., and Rao, S. V. B.: Differences in the  
462 climatological characteristics of precipitation between active and break spells of the  
463 Indian summer monsoon, *J. Clim.*, 29, 7797-7814, 2016.
- 464 Remer, L., Kaufman, Y., Tanré, D., Mattoo, S., Chu, D., Martins, J., Li, R., Ichoku, C.,  
465 Levy, R., Kleidman, R., Eck, T., Vermote, E., and Holben, B.: The MODIS aerosol  
466 algorithm, products, and validation, *J. Atmos. Sci.*, 62, 947–973, 2005.
- 467 Romatschke, U., Medina, S., and Houze, R. A.: Regional, seasonal, and diurnal variations of  
468 extreme convection in the South Asian region, *J. Clim.*, 23, 419–439, 2010.
- 469 Rosenfeld, D., et al.: Global observations of aerosol-cloud-precipitation-climate interactions,  
470 *Rev. Geophys.*, 52, 750-808, doi:10.1002/2013RG000441, 2014.
- 471 Roxy, M.: Sensitivity of precipitation to sea surface temperature over the tropical summer  
472 monsoon region—and its quantification, *Clim. Dyn.*, 43, 1159-1169, 2014.
- 473 Roxy, M., Tanimoto, Y., Preethi, B., Terray, P., and Krishnan, R.: Intraseasonal SST-  
474 precipitation relationship and its spatial variability over the tropical summer monsoon  
475 region, *Clim. Dyn.*, 41, 45-61, 2013.
- 476 Sabin, T., Babu, C., and Joseph, P.: SST–convection relation over tropical oceans, *Int. J.*  
477 *Climatol.* 33, 1424–1435, 2012.
- 478 Saikranthi, K., Rao, T. N., Radhakrishna, B., and Rao, S. V. B. : Morphology of the vertical  
479 structure of precipitation over India and adjoining oceans based on long-term



- 480 measurements of TRMMPR, *J. Geophys. Res. Atmos.*, 119, 8433–8449, doi:  
481 10.1002/2014JD021774, 2014.
- 482 Saikranthi, K., Radhakrishna, B., Satheesh, S. K., and Rao, T. N.: Spatial variation of  
483 different rain systems during El Niño and La Niña periods over India and adjoining  
484 ocean, *Clim. Dyn.*, 50, 3671–3685, doi: 10.1007/s00382-017-3833-4, 2018.
- 485 Satheesh, S. K., Moorthy, K. K., Kaufman, Y. J., and Takemura, T.: Aerosol Optical depth,  
486 Physical properties and Radiative forcing over the Arabian Sea, *Meteorol. Atmos.*  
487 *Phys.*, 91, 45–62, doi:10.1007/s00703-004-0097-4, 2006.
- 488 Schumacher, C. and Houze, R. A.: Comparison of radar data from the TRMM satellite and  
489 Kwajalein oceanic validation site. *J. Appl. Meteor.*, 39, 2151–2164, 2000.
- 490 Schumacher, C. and Houze, R. A.: Stratiform rain in the tropics as seen by the TRMM  
491 precipitation radar, *J. Climate.*, 16, 1739–1756, 2003.
- 492 Sengupta, D., Goswami, B. N., and Senan, R.: Coherent intraseasonal oscillations of ocean  
493 and atmosphere during the Asian summer monsoon, *Geophys. Res. Lett.*, 28, 4127–  
494 4130, 2001.
- 495 Shenoi, S. S. C., Shankar, D., and Shetye, S. R.: Differences in heat budgets of the near-  
496 surface Arabian Sea and Bay of Bengal: Implications for the summer monsoon, *J.*  
497 *Geophys. Res.*, 107(C6), 3052, doi:10.1029/2000JC000679, 2002.
- 498 Sunilkumar, K., Rao, T. N., Saikranthi, K., and Rao, M. P.: comprehensive evaluation of  
499 multisatellite precipitation estimates over India using gridded rainfall data, *J. Geophys.*  
500 *Res. Atmos.*, 120, doi:10.1002/2015JD023437, 2015.
- 501 Tao, W.-K., et al.: Retrieval of latent heating from TRMM measurements, *Bull. Am.*  
502 *Meteorol. Soc.*, 87, 1555–1572, 2006.



503 Tao, W.-K., Chen, J.-P., Li, Z., Wang, C., and Zhang, C.: Impact of aerosols on convective  
504 clouds and precipitation, *Rev. Geophys.*, 50, RG2001, doi:10.1029/2011RG000369,  
505 2012.

506 Twomey, S.: The influence of pollution on the short wave albedo of clouds, *J. Atmos. Sci.*,  
507 34, 1149–1152, 1977.

508 Wang, B., Ding, Q., Fu, X., Kang, I.-S., Jin, K., Shukla, J., and Doblas-Reyes, F.:  
509 Fundamental challenge in simulation and prediction of summer monsoon rainfall,  
510 *Geophys. Res. Lett.*, 32, L15711, doi:10.1029/2005GL022734, 2005.

511 Wood, R., and Bretherton, C. S.: On the relationship between stratiform low cloud cover and  
512 lower-tropospheric stability, *J. Clim.*, 19, 6425–6432, 2006.

513 Woolnough, S.J., Slingo, J.M., and Hoskins, B.J.: The relationship between convection and  
514 sea surface temperature on intraseasonal timescales, *J. Climate*, 13, 2086–2104, 2000.

515 Wu, R., and Kirtman, B. P.: Roles of Indian and Pacific Ocean air–sea coupling in tropical  
516 atmospheric variability, *Clim. Dyn.*, 25(2–3), 155–170, 2005.

517 Yoneyama, K., Zhang, C., and Long, C. N.: Tracking pulses of the Madden–Julian  
518 oscillation, *Bull. Amer. Meteor. Soc.*, 94, 1871–1891, [https://doi.org/10.1175/BAMS-](https://doi.org/10.1175/BAMS-D-12-00157.1)  
519 [D-12-00157.1](https://doi.org/10.1175/BAMS-D-12-00157.1), 2013.

520

521

522

523

524

525

526

527



528

### Figure captions

529 **Figure 1:** Spatial distribution of SWM mean SST (in °C) obtained from ERA-Interim  
530 reanalysis data over the AS and the BOB. The regions considered in this analysis over  
531 these two seas are shown with the boxes.

532 **Figure 2:** (a) and (b) represent the altitudinal distribution of occurrence of conditional  
533 reflectivity ( $\geq 17$  dBZ) as a function of SST with respect to precipitation occurrence at  
534 that particular SST interval over the AS and the BOB, respectively.

535 **Figure 3:** (a), (d) and (b), (e) represent vertical profiles of median reflectivity and their  
536 standard deviation (in dBZ) with SST over the AS (63°E-72°E & 8°N-20°N) and the  
537 BOB (83°E-92°E & 8°N-21°N), respectively during the SWM season. (c) and (f)  
538 show the number of conditional reflectivity pixels at each altitude used for the  
539 estimation of the median and standard deviation.

540 **Figure 4:** The variation of mean LTS with SST over the AS (63°E-72°E & 8°N-20°N) and  
541 the BOB (83°E-92°E & 8°N-21°N) during the SWM season.

542 **Figure 5:** (a) and (b), respectively, represent the variation of mean CER ice (in  $\mu\text{m}$ ) and  
543 mean CER liquid (in  $\mu\text{m}$ ) with SST over the AS (63°E-72°E & 8°N-20°N) and the  
544 BOB (83°E-92°E & 8°N-21°N) during the SWM season.

545 **Figure 6:** (a) The variation of mean AOD and (b) TCWV (in mm) with SST over the AS  
546 (63°E-72°E & 8°N-20°N) and the BOB (83°E-92°E & 8°N-21°N) during SWM.

547 **Figure 7:** Winds during the SWM season at 850 hPa and 500 hPa levels. The shading colors  
548 represent the magnitude of the wind and arrow indicates the direction of the wind.

549 **Figure 8:** Latitudinal variation (for every 2° latitude interval) of mean aerosol optical depth  
550 over Arabian Sea averaged over 63-72°E.

551

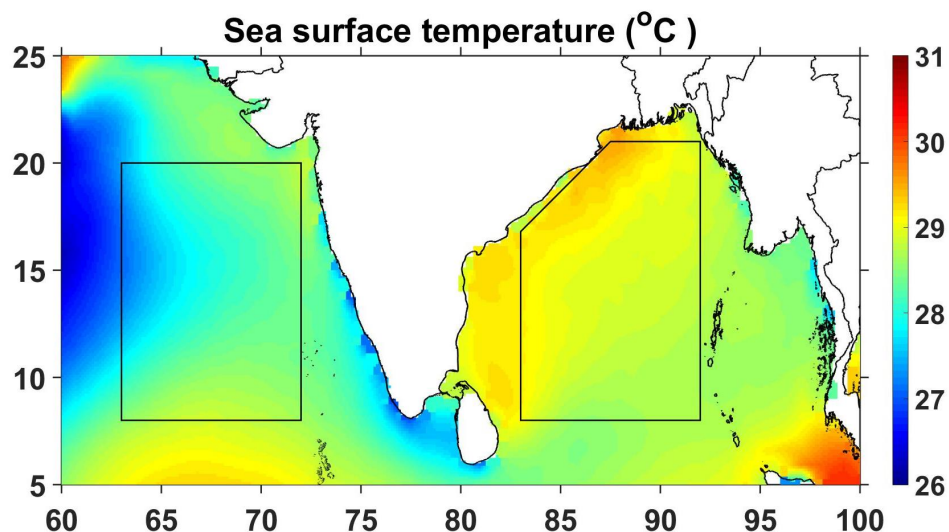
552



553

### Figures

554



555

**Figure 1:** Spatial distribution of SWM mean SST (in °C) obtained from ERA-Interim reanalysis data over the AS and the BOB. The regions considered in this analysis over these two seas are shown with the boxes.

559

560

561

562

563

564

565

566

567

568

569

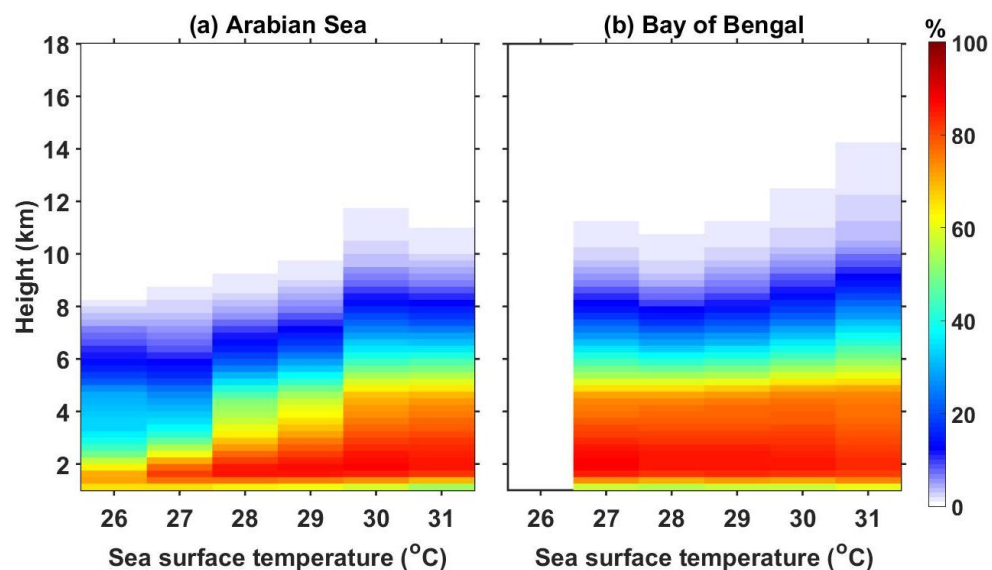
570

571

572

573

574



575

576

577 **Figure 2:** (a) and (b) represent the altitudinal distribution of occurrence of conditional  
578 reflectivity ( $\geq 17$  dBZ) as a function of SST with respect to precipitation occurrence at  
579 that particular SST interval over the AS and the BOB, respectively.

580

581

582

583

584

585

586

587

588

589

590

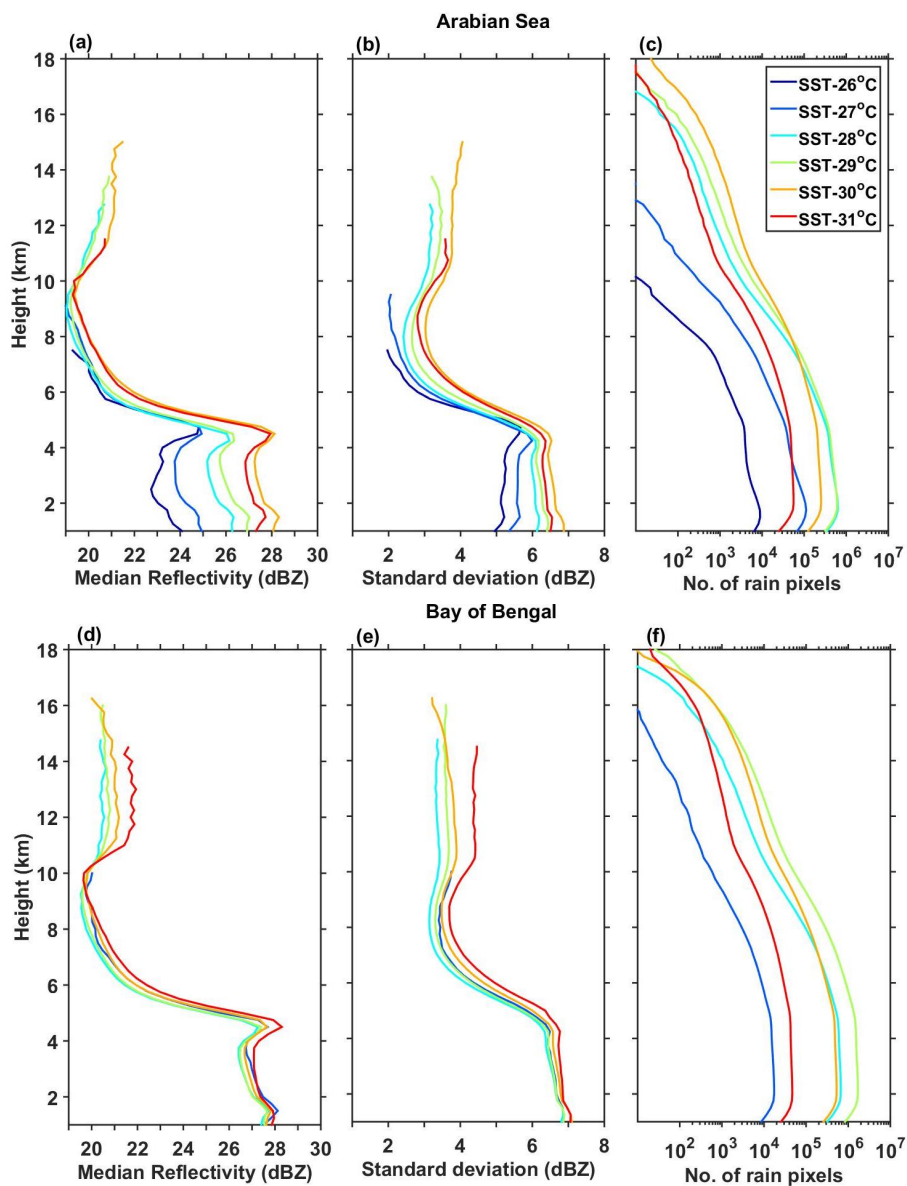
591

592

593

594

595

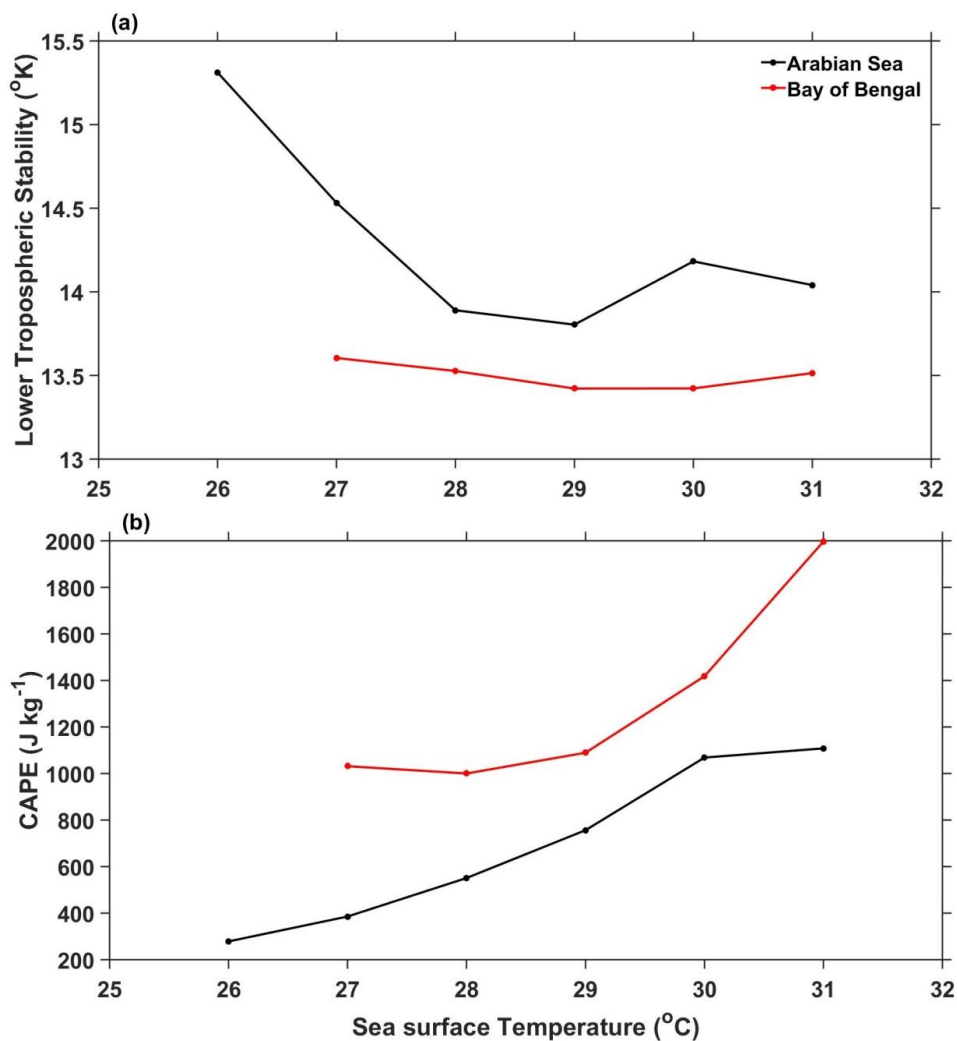


597 **Figure 3:** (a), (d) and (b), (e) represent vertical profiles of median reflectivity and their  
598 standard deviation (in dBZ) with SST over the AS (63°E-72°E & 8°N-20°N) and the  
599 BOB (83°E-92°E & 8°N-21°N), respectively during the SWM season. (c) and (f)  
600 show the number of conditional reflectivity pixels at each altitude used for the  
601 estimation of the median and standard deviation.

602

603

604



605

606

607 **Figure 4:** (a) The variation of mean LTS (in  $^{\circ}\text{K}$ ) with SST over the AS ( $63^{\circ}\text{E}$ - $72^{\circ}\text{E}$  &  $8^{\circ}\text{N}$ -  
608  $20^{\circ}\text{N}$ ) and the BOB ( $83^{\circ}\text{E}$ - $92^{\circ}\text{E}$  &  $8^{\circ}\text{N}$ - $21^{\circ}\text{N}$ ) during the SWM season. (b) Same as  
609 (a) but for CAPE.

610

611

612



613

614

615

616

617

618

619

620

621

622

623

624

625

626

627

628

629

630

631

632

633

634

635

636

637

638

639

640

641

642

643

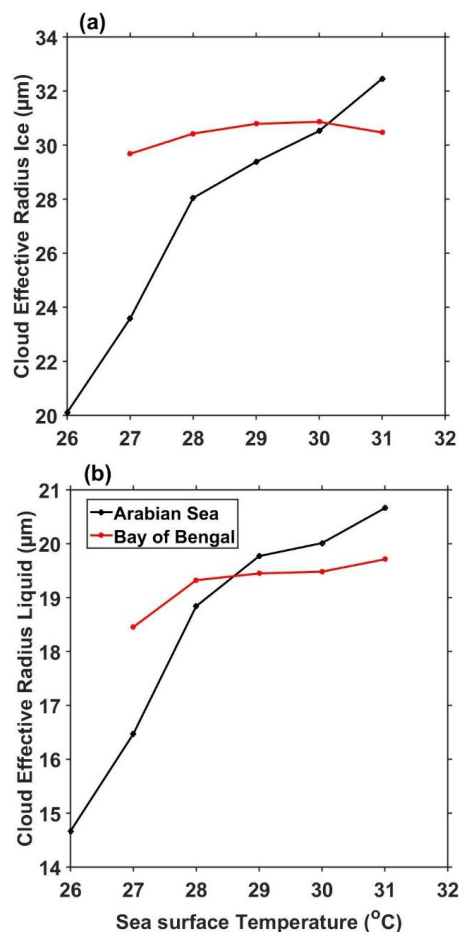
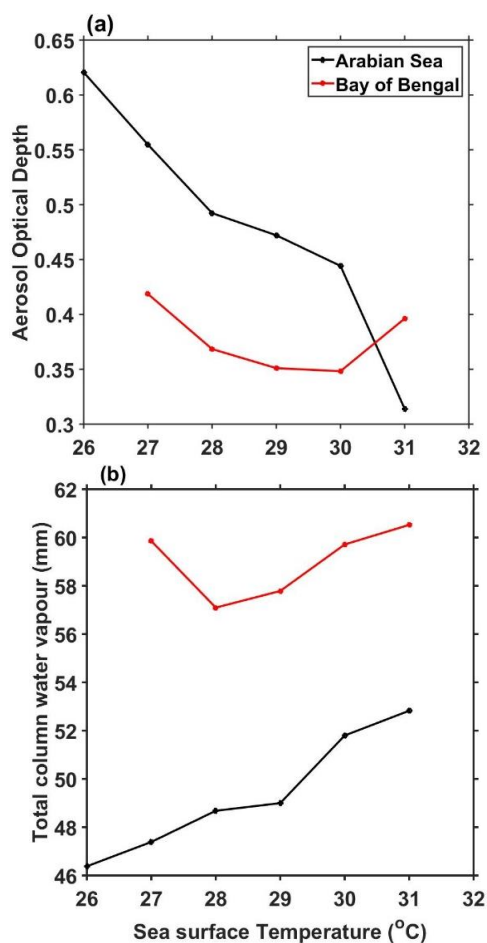


**Figure 5:** (a) and (b), respectively, represent the variation of mean CER ice (in  $\mu\text{m}$ ) and mean CER liquid (in  $\mu\text{m}$ ) with SST over the AS ( $63^{\circ}\text{E}$ - $72^{\circ}\text{E}$  &  $8^{\circ}\text{N}$ - $20^{\circ}\text{N}$ ) and the BOB ( $83^{\circ}\text{E}$ - $92^{\circ}\text{E}$  &  $8^{\circ}\text{N}$ - $21^{\circ}\text{N}$ ) during the SWM season.

644

645



665 **Figure 6:** (a) The variation of mean AOD and (b) TCWV (in mm) with SST over the AS  
666 (63°E-72°E & 8°N-20°N) and the BOB (83°E-92°E & 8°N-21°N) during SWM.

667

668

669

670

671

672

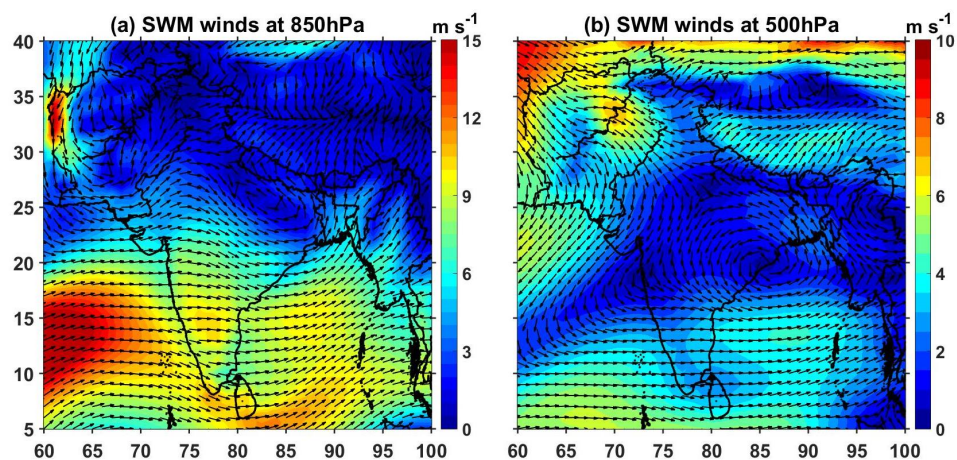
673

674



675

676



677

678 **Figure 7:** Winds during the SWM season at 850 hPa and 500 hPa levels. The shading colors  
679 represent the magnitude of the wind and arrow indicates the direction of the wind.

680

681

682

683

684

685

686

687

688

689

690

691

692

693

694

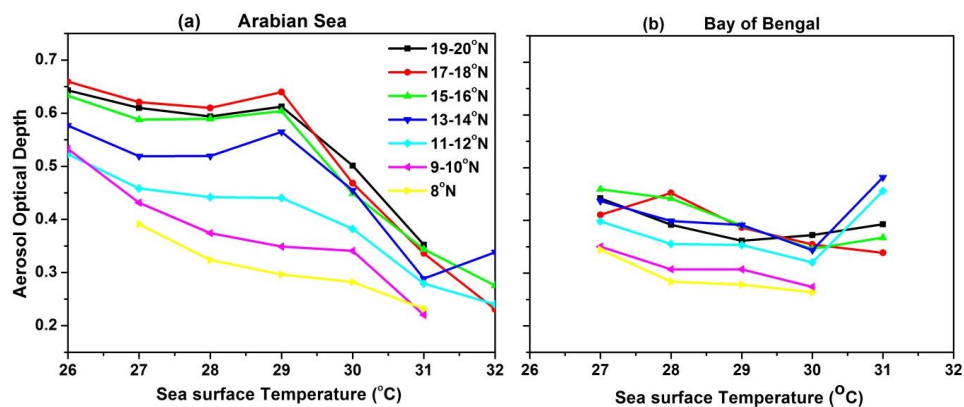
695

696



697

698



699

700 **Figure 8:** (a) and (b), respectively, represent latitudinal variation (for every 2° latitude  
701 interval) of mean AOD over the AS (between 63°E and 72°E) and the BOB (between  
702 83°E and 92°E).